Applied Nanoscience
https://doi.org/10.1007/s13204-020-01606-5

ORIGINAL ARTICLE

Facile synthesis of new composite, Ag-Nps-loaded core/shell CdO/Co_3O_4 NPs, characterization and excellent performance in antibacterial activity

A. M. Nassar[1,2] · Z. A. Alrowaili[3] · Ahmed A. M. Ahmed[4,5] · B. A. Cheba[6,7] · Sultan Akhtar[8]

Received: 11 August 2020 / Accepted: 23 October 2020

Abstract

Here, we report for the first time the synthesis of new composite Ag-NPs-loaded core/shell mixed oxides NPs, CdO/Co_3O_4. First, nano-precursors (1) and (2) consist of mixed (cadmium oxalate/cobalt oxalate) and (silver oxalate/cadmium oxalate/cobalt oxalate), respectively, have been synthesized and characterized. Then, thermal treatment of 1 and 2 at 400 °C resulted in the formation of composites CdO/Co_3O_4 (3) and Ag-NPs@CdO/Co_3O_4 (4), respectively. The materials have been characterized by IR, SEM, TEM, TGA and XRD. The morphologies of the materials were described from SEM images. TEM images revealing the formation of core–shell structure with average particles size 5–20 nm. The crystal sizes were calculated from XRD patterns and resulted in 14.21, 14.65, 15.06 and 15.79 nm for 1, 2, 3 and 4, respectively. All the materials undergo tests as antibacterial agents against Gram-positive bacteria (*Bacillus subtilis* and *Enterococcus spp*.) and Gram-negative bacteria (*E. coli* and *Pseudomonas aeruginosa*). Precursor 2 and composite 4 impart higher inhibition against all the bacterial strains compared to precursor 1 and composite 3.

Keywords Mixed oxides · Cadmium · Cobalt · Ag-NPs · Composite · Antibacterial

Introduction

Metal oxides nanomaterials are well-known components for different applications (Bayal and Jeevanandam 2012). The main attention of these materials resulted from their heightened electronic, optical, magnetic, chemical and physical properties than their bulk counter parts (Yuan et al. 2014). Mixed metal oxides are subjected in different areas such as superconductors (Williams et al. 1988), photocatalysts (Koohestani 2019), sensors (Zakrzewska 2001), groundwater remediation (Basu and Ghosh 2013), removal of air toxicity (Li et al. 2011) and pharmaceuticals (Abureesh et al. 2018).

As a significant n-type semiconductor metal-oxide, cadmium oxide (CdO) which has a direct band gap 1.3–2.5 eV (Balamurugan et al. 2016). CdO is included in several applications such as electrical, antibacterial, medical and optical fields (Manjula et al. 2015). Recently, a composite of glucose/cadmium oxide nanoparticles was fabricated and showed potential therapeutic value as an effective anti-glycation agent (Zahera et al. 2020). Gadolinium-doped cadmium oxide thin films were prepared and showed high-performance optoelectronic properties with high-transmittance in visible light (Sakthivel

✉ A. M. Nassar
amnassar@ju.edu.sa

1 Department of Chemistry, College of Science, Jouf University, Sakaka, Saudi Arabia

2 Department of Chemistry, Faculty of Science, Al-Azhar University, Nasr-City, Cairo, Egypt

3 Department of Physics, College of Science, Jouf University, Sakaka, Saudi Arabia

4 Department of Basic Science, Common First Year Deanship, Jouf University, Sakaka, Saudi Arabia

5 Department of Chemistry, Faculty of Science, Cairo University, Giza, Egypt

6 Department of Biology, College of Science, Jouf University, Sakaka, Saudi Arabia

7 Department of Biotechnology, College of Nature and Life Sciences, University of Science and Technology of Oran Mohamed-Boudiaf (USTOMB), BP 1505 Al Mnaouar, 31000 Oran, Algeria

8 Department of Biophysics, Institute for Research and Medical Consultations (IRMC), Imam Abdulrahman Bin Faisal University, P. O. Box. 1982, Dammam 31441, Saudi Arabia

Published online: 09 November 2020

et al. 2020). A composite of cadmium oxide@graphene was synthesized via a green route based on onion extracts. The nanocomposite imparted antibacterial activity higher than that of pure CdO NPs (Sadhukhan et al. 2019). A. Salem studied the fabrication of silver nanoparticles-doped cadmium oxide composite with face-centered cubic structure and its optical properties. The study demonstrated that the composite present a promising candidate for optoelectronic devices (Salem 2014).

Spinel cobalt oxide, Co_3O_4 is known as a magnetic p-type semiconductor material with unique shape (Salam et al. 2020). It is environment-friendly and has excellent chemical and physical stability (Vennela et al. 2019). It is widely studied as promising materials for several applications including the medical nanotechnology and biotechnology, photocatalytic degradation of organic pollutants, electrochemistry, lithium-ion batteries, gas sensors, and energy storage devices (Assim et al. 2017).

Loading of silver nanoparticles, Ag-NPs on the materials surface or doping in their crystalline matrix significantly impacts on the development of the materials physical and chemical properties (Nassar et al. 2018). Among the activities of Ag-NPs, their antimicrobial activity and high sterilization performance are widely well discussed (Ren et al. 2019; Gong et al. 2007; Kooti et al. 2013). The action mechanism of the Ag-NPs antibacterial activity explained by their high permeability through the bacteria cell wall membrane due to Ag-NPs has a small size as well as their large specific surface area (Liu et al. 2013).

According to the best of our knowledge, recently, only one work has reported the fabrication and characterization of CdO/Co_3O_4 composite for the first time via a simple solvothermal method (Wang et al. 2020). In this work and based on the biological potential of CdO, Co_3O_4, and Ag-NPs, our focus is to fabricate, characterize and study the antibacterial activity of mixed oxides CdO/Co_3O_4 and its loaded silver nanoparticles novel composite Ag-NPs@CdO/Co_3O_4.

Experimental

Materials and reagents

The materials that were used in this work without involving any purification are cadmium nitrate tetrahydrate, cobalt nitrate hexahydrate, silver nitrate and oxalic acid dihydrate from Sigma-Aldrich (USA). Milli-Q water was used in all experiments.

Synthesis of mixed cadmium oxalate/cobalt oxalate (precursor 1)

To aqueous mixed solutions of cadmium nitrate tetrahydrate (3.085 g, 0.01 mol), and cobalt nitrate hexahydrate (2.910 g, 0.01 mol), an aqueous solution of oxalic acid dehydrate as precipitant (2.52 g, 0.02 mol) was added with continues stirring. A pink precipitate was formed after 1 min from addition. After stirring for 2 h at 80 °C, it was filtered, washed with hot water and acetone several times before being dried using a dry furnace at 110 °C. Precursor 1 was stored in a desiccator until used.

Synthesis of mixed silver oxalate/cadmium oxalate/cobalt oxalate (precursor 2)

To aqueous mixed solutions of silver nitrate (3.4 g, 0.02 mol), (3.085 g, 0.01 mol), and cobalt nitrate (2.910 g, 0.01 mol), an aqueous solution of the oxalic acid as precipitant (3.78 g, 0.03 mol) was added under continues stirring. A pale pink precipitate was formed immediately and then stirred for 2 h at 80 °C. Then, the solid formed was filtered, washed with hot water and acetone several times, and dried using a dry furnace at 110 °C. Precursor 2 was stored in a desiccator until used.

Fabrication of CdO/Co_3O_4 (3) and Ag-NPs@CdO/Co_3O_4 (4)

Composites 3 and 4 were fabricated via the thermal degradation of precursors 1 and 2, respectively. 1 g from precursor in porcelain mortar was stated in muffle furnace at 400 °C with heating rate 10 °C/min, then kept 2 h at this degree to remove the crystalline water and oxalate residues. A black powder of composite 3 (0.45 g, 97.83% yield) and deep gray powder of composite 4 (0.50 g, 94.33% yield) were formed and kept in a desiccator until used.

Instrumentation

SEM images were detected by Thermo Scientific Quattro S. FT-IR spectra were measured by IRTracer-100 SHIMADZU spectrophotometer. X-ray patterns were recorded using XRD-7000 SHIMADZU, with a CuKα1 radiation source. TGA measurements were performed using TGA-51SHIMADZU with a heating rate of 10 °C/min. TEM images were recorded using (FEI, Morgagni, 268 at 80 keV) analysis with dispersion in ethanol and deposited onto the TEM grids having carbon support.

Antibacterial experiments

The antibacterial activity of the materials 1–4 were deterimened using agar-well diffusion method (Perez 1990). In summary, the bacterial isolates have been cultivated using a nutrient broth medium that contained 5 g/L of yeast extract, 10 g/L bactotryptone and 10 g/L NaCl for 18 h at 37 °C using sterile cotton swabs in a sterile condition; each

bacterial strain was uniformly swabbed onto separate agar plates, and the agar media were punched using 8-mm-diameter wells and filled with 500 ul of nanoparticles aqueous solutions. The plates were, then, refrigerated for 2 h before being incubated at 37 °C for 24 h., where the antibacterial activity of the samples could be accessed by measuring the diameter of growth prevention halo (zone of inhibition). The tested Bacteria were *Bacillus subtilis* (A), *Enterococcus sp.* (B), *E.coli* (C), *and Pseudomonas aerogenosa* (D).

Results and discussion

In this work, a composite of core–shell mixed oxides CdO/Co_3O_4 and its loaded silver nanoparticles new composite are fabricated by thermal degradation of the corresponding mixed oxalate precursors, schemes 1, 2. Several physicochemical techniques have been used to characterize the materials. The antibacterial activity of precursors and composites has been studied.

Materials characterization

TGA analysis

The thermal gravimetric analysis of 1 and 2 were investigated, Fig. 1 to assess the suitable temperature required for conversion of precursors 1 and 2 to composites 3 and 4 and to estimate the composition of the formed residues after thermal degradation. The samples were heated from 25 to 600 °C with heating rate 10 °C/min. The precursors are stable up to ≈ 180 °C indicating the absence of adsorbed water molecules. Curve (TG) of precursor 1, ($CdC_2O_4.3H_2O + 3CoC_2O_4.2H_2O$), Fig. 1a represents two steps of decomposition in the range 180–390 °C with mass loss 54.10% which is close to the theoretical value. The residual part 45.90% corresponds to the successful formation of CdO/Co_3O_4. Figure 1b shows the thermograms of precursor 2, ($CdC_2O_4.3H_2O + 3CoC_2O_4.2H_2O + Ag_2C_2O_4$). Two degradation steps in the range 180–315 °C with mass loss 43.50% leaving residual part 46.50% which agreed well with the theoretical calculations for the formation of 2Ag/CdO/Co_3O_4.

FT-IR spectroscopy

Figure 2a–d shows the FT-IR spectra of materials 1–4, respectively. The precursors FT-IR spectra match the findings of previous studies on the oxalate salts (Nayaka et al. 2016). Figure 2a shows band ~ 3350 cm^{-1} which was assigned to νO–H of crystalline water molecules (Elseman et al. 2017).The oxalate molecules exhibit transmittance at 1625, 1310, 830 cm^{-1} which are characteristics of bending and stretching vibrations of O–C–O oxalate moiety (Sun and Qiu 2012).The two bands in the far infrared region at 492 and 435 cm^{-1} may be assignable to νCo–O and νCd–O, respectively. Figure 2b exhibits the same bands observed in Fig. 2a as well as the new one at 520 cm^{-1} which could be a result of the ν O–Ag (Nassar et al. 2018). Figure 2c, d shows the FT-IR spectra of composites 3 and 4, respectively. Two apparent and sharp bands at 540–550 cm^{-1} and 640–650 cm^{-1} are characteristic of ν_1 and ν_2 for spinel Co_3O_4, respectively. (Makhlouf et al. 2013). The first band was due to cobaltic oxide vibration in the octahedral hole, and the second band was assigned to cobaltous oxide vibration in the tetrahedral hole in the spinel Co_3O_4 lattice (Fouad et al. 2011). The spectra exhibit a strong band at 750 cm^{-1}. This band is assignable to Cd–O stretching vibration (Małecka and Łącz 2008). No absorptions around 3400 and 1680 cm^{-1} which assignable to H_2O stretching and

Scheme 1 Fabrication of composite 3 from precursor 1

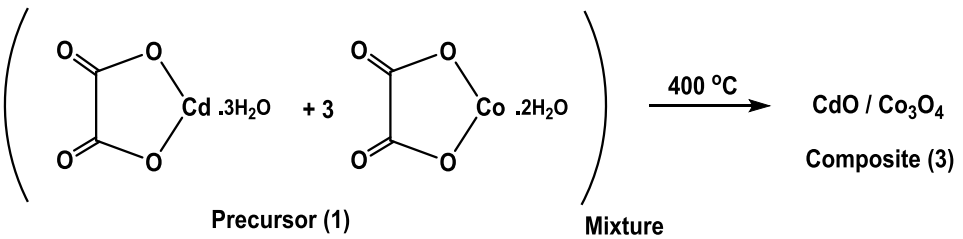

Scheme 2 Fabrication of composite 4 from precursor 2

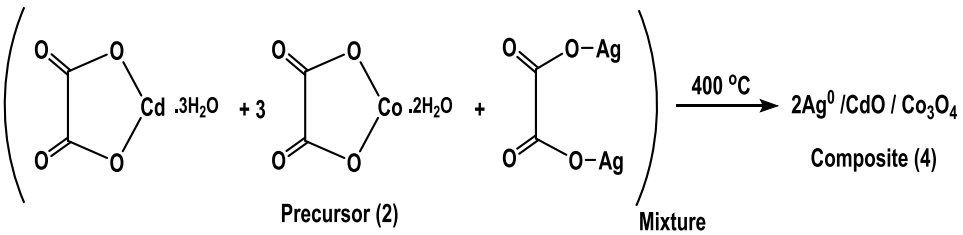

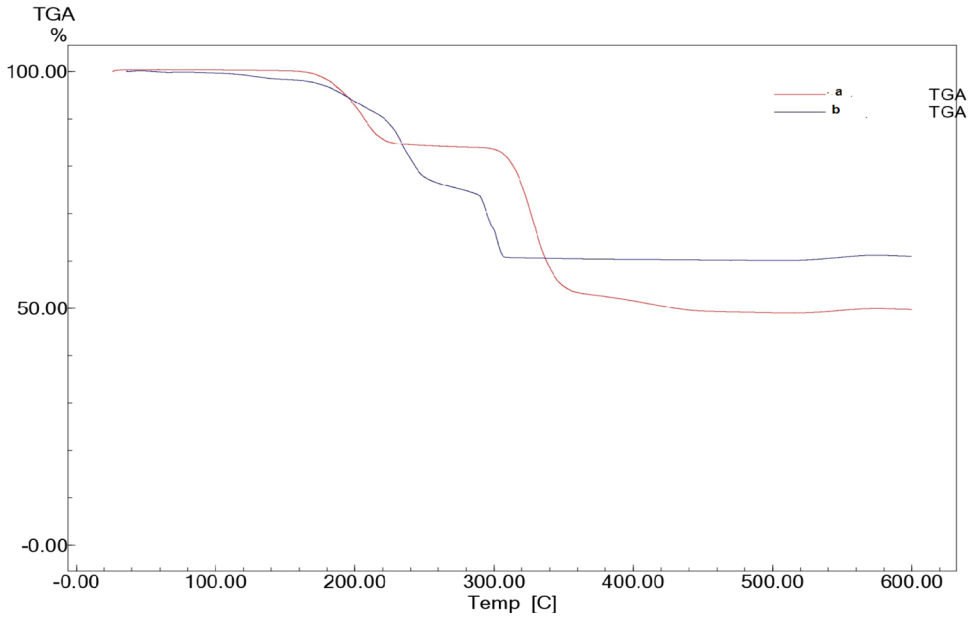

Fig. 1 TGA of precursors 1 (**a**) and 2 (**b**)

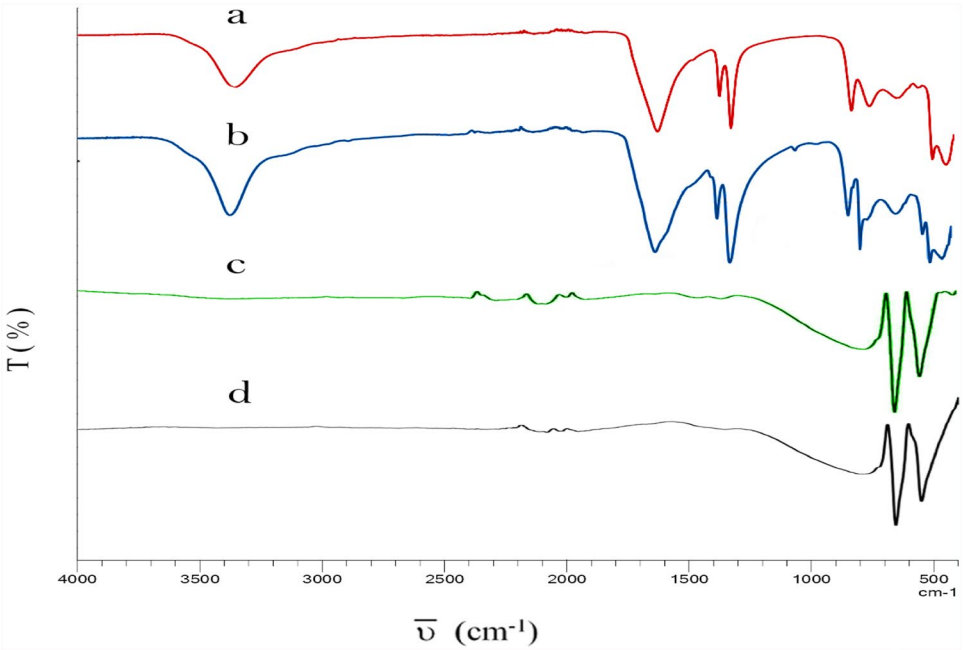

Fig. 2 FT-IR spectra of precursor 1 (**a**), precursor 2 (**b**), composite 3 (**c**) and composite 4 (**d**)

bending vibrations, respectively, indicating the absence of chemically or physically bonded water molecules in composites structures (Zou et al. 2008).

XRD analysis

Figure 3a–d shows the XRD diffractogram of precursors and their thermal decomposition products. Figure 3a exhibits the characteristic peaks of cobalt oxalate (Du et al. 2010) and cadmium oxalate (Raj et al. 2008). The peaks at $2\theta = 18.75°$, 22.65°, 30.15° and 44.50 ° are due to (202), (004), (400) and (224) crystallographic planes which can be indexed as β-$CoC_2O_4.2H_2O$. The peaks observed at $2\theta = 18.95°$, 24.48°, 30.20°, 33.60°, 39.70°, 44.56° and 47. 75° are referring to planes (111), (012), (200), (210), (213), (030) and (302) indicating the formation of hydrated cadmium oxalate crystals. The main XRD patterns of silver oxalate appeared at $2\theta = 17.10°$,

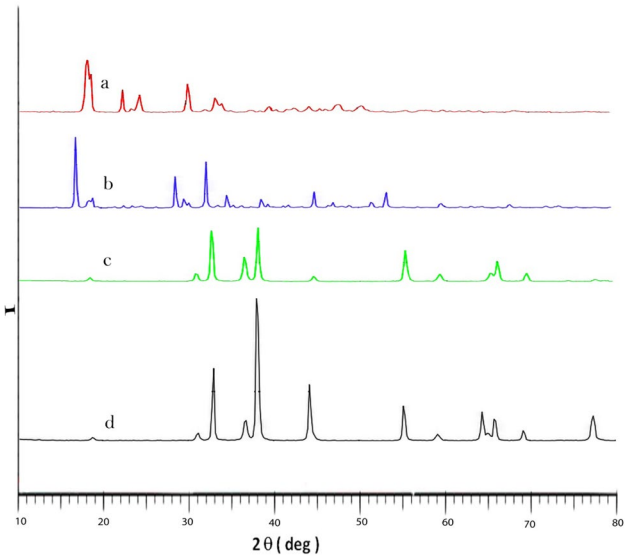

Fig. 3 XRD patterns of precursor 1 (**a**), precursor 2 (**b**), composite 3 (**c**) and composite 4 (**d**)

19.05°, 28.78°, 29.91°, 32.18°, 36.45°, 38.79°, 39.45°, 47.10°, 51.59° and 67.55°. The X-ray data are in good agreement with the JCPDS No.022-1335 for silver oxalate (Yang et al. 2018). In Fig. 3c, the detected peaks are related to CdO and spinel Co_3O_4 phases. The peaks located at $2\theta = 18.90°$, 31.15°, 36.50°, 44.90°, 55,55°, 59.30° and 65.33° are assigned to diffraction patterns of crystallographic planes (111), (220), (311), (400), (422), (511), and (440), respectively. All peaks are well matched for Co_3O_4 phase (JCPDS No:76–1802) (Li et al. 2008).The strong diffraction peaks at 2θ values of 33.05°, 38.45°, 65.90° and 69.24° correspond to the (111), (200), (311) and (222) planes, respectively. These peaks were indexed to a cubic CdO pattern (JCPDS card no.65-2908) (Usharani et al. 2015).Same peaks of CdO and Co_3O_4 are observed in Fig. 3d as well as the characteristic peaks of silver nanoparticles corresponding to (111), (200), (220), and (311) planes were observed at 2θ values of 38.14, 44.35, 65.00, and 77.5, respectively (Nassar et al. 2019).No diffraction peaks resulted from the CoO or the metallic cobalt were detected confirming the obtained product from thermal decomposition is pure Co_3O_4 phase. The average crystalline size of each material was calculated using the Scherrer Eq. (1) (Abo Zeid et al. 2020,2019):

$$D = \frac{K\lambda}{\beta \cos\theta} \quad (1)$$

where D is the average particle size, λ is the alpha radiation wavelength of Copper K, β is the whole width of the diffraction peak, $k = 0.9$ is the shape-sensitive coefficient and θ is the diffraction angle. The average crystalline size was found to be 14.21, 14.65, 15.06 and 15.79 nm for materials 1, 2, 3 and 4, respectively. According to G. Gomes et al., silver loading results in larger and more particle sizes (Gomes et al. 2018).

Morphological studies

SEM and TEM images of materials were captured and collected in Fig. 4a–d and Fig. 5a–h, respectively. The morphologies of the precursors 1 and 2 show the elongated rod particle shape of cobalt and cadmium oxalates, columnar morphology of silver oxalate and nanosphere of silver ions. The composites 3 and 4 show nanocrystaliine structure of CdO/Co_3O_4. In precursor 2 and composite 4 images, the silver nanospheres show physically and uniformly surface dispersion. TEM images of the materials show the average particles size 5–20 nm which was nearly in consonance with the crystals size obtained from XRD. Composites 3 shows core–shell structure as $CdO@Co_3O_4$. Composite 4 shows the mixed oxides core–shell structure is enveloped with Ag-Nps as $Ag@CdO/Co_3O_4$. The photos of precursor 2 and composite 4 reveal that the silver particles are predominantly spherical and circular and not physically in contact with each other.

Antibacterial activity

The antibacterial results are provided in Table.1 and illustrated in Figs. 6, 7. The results showed generally that all tested materials exhibited high antibacterial activity following the order 2 > 4 > 1 > 3 in comparison to both Gram-positive and -negative bacteria. The precursor 2 and composite 4 displayed the higher bacterial growth reduction expressed as larger growth inhibition zone diameter (mm); this stranger antibacterial potential may be due to the presence of silver in their structure.

The most affected bacterial species by the tested nanocomposites were determined to be in the following descending order *Enterococcus sp.* > *E. coli* > *Bacillus subtilis* > and *Pseudomonas aeruginosa.* Similar results obtained showed that CdO NPs and Co_3O_4 NPs exhibited high antibacterial activity (Sadhukhan et al. 2019; Elango et al. 2018). Co_3O_4 and CdO NPs antibacterial activity might be due to generating the reactive oxygen species (ROS) from the surface of NPs that reacted and destroyed the bacterial cell structure. The higher antibacterial potential of silver containing materials might be due to their structural morphology and high

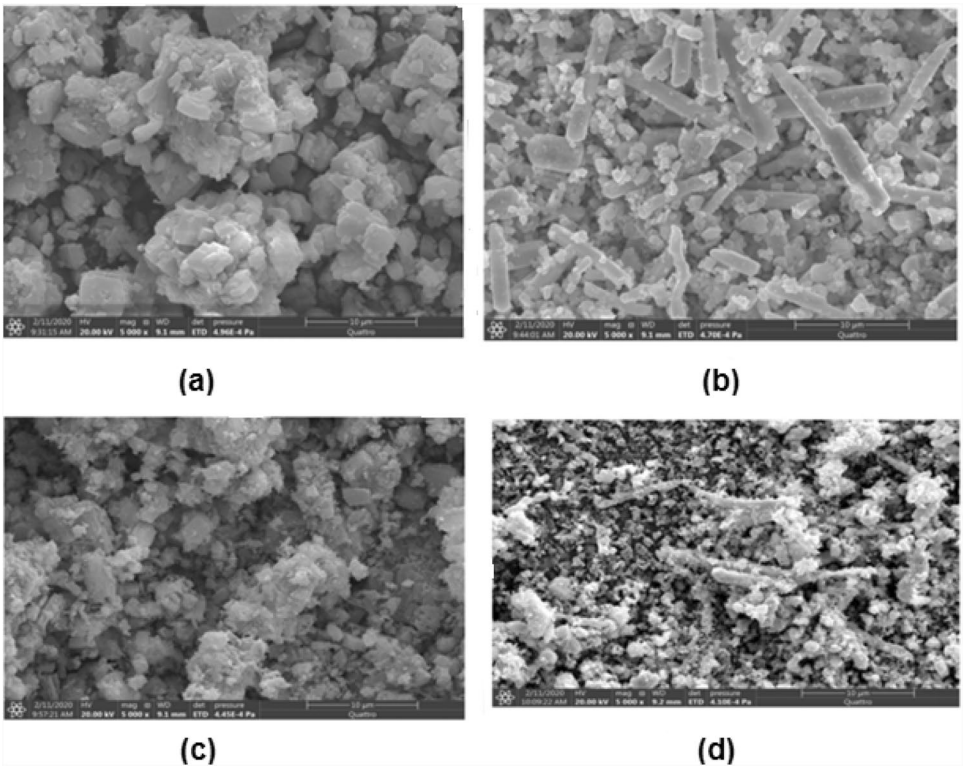

Fig. 4 SEM images of precursor 1 (**a**), precursor 2 (**b**), composite 3 (**c**) and composite 4 (**d**)

surface area, which apparently well interacted with bacteria and provided a better superficial release of the reactive oxygen species (Morones et al. 2005; Rai et al. 2012).

To sum up, the analysis proved that the precursor and composite supplemented with silver were significantly efficient regarding inactivating some human bacterial pathogens.

The minimum inhibitory concentration (MIC) values of 2 and 4 at different concentration 0.08, 0.16, 0.32 and 0.64 µg/mL, were recorded by standard serial dilution method against *Bacillus subtilis and E. coli* using disk diffusion technique (Alsohaimi et al. 2020). The results are summarized in Table 2 and illustrated in Fig. 8. The precursor 2 exhibited the higher antibacterial potential compared to composite 4 expressed as larger inhibition zone diameter (mm), whereas the MIC was found to be 0.08 and 0.32 µg/mL for 2 and 4, respectively.

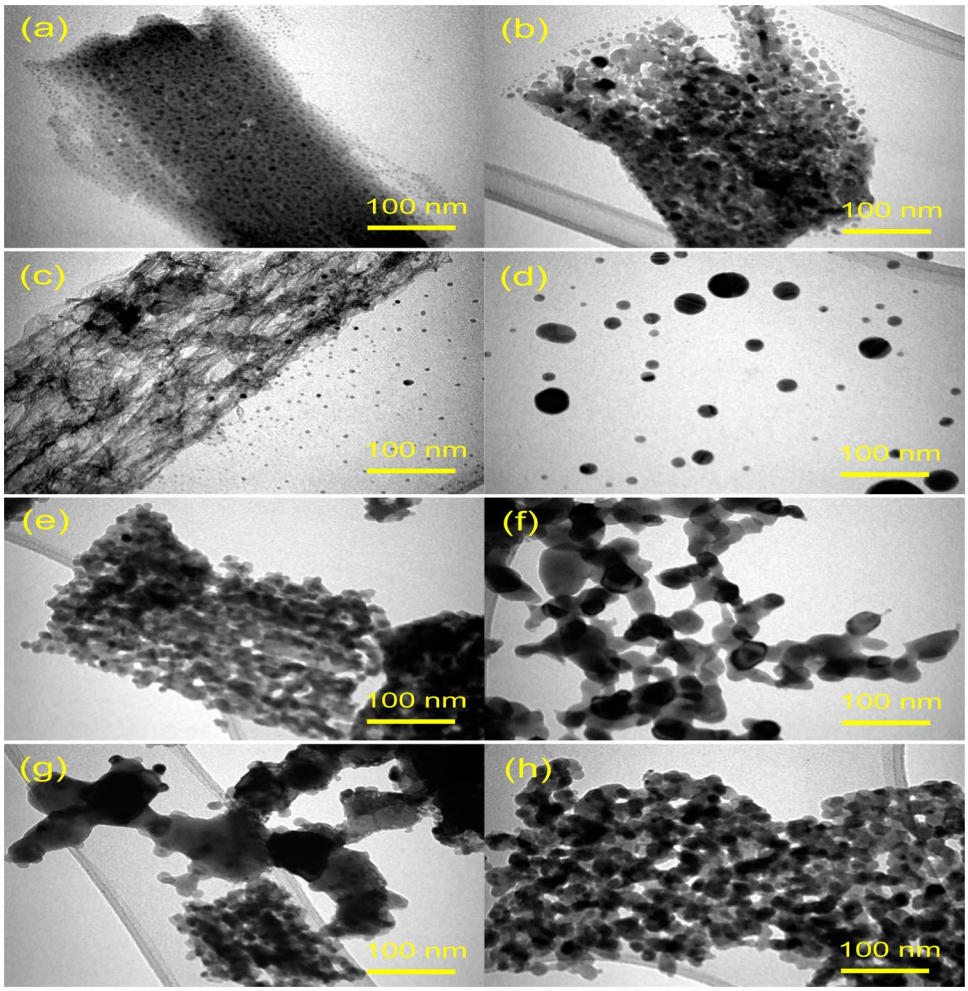

Fig. 5 TEM images (**a**, **b**) precursor 1, **c**, **d** precursor 2, **e**, **f** composite 3 and **g**, **h** composite 4

Table 1 Antibacterial activity of materials 1, 2, 3, 4 tested against *Bacillus subtilis* (A), *Enterococcus sp.* (B), *E. coli* (C), *and Pseudomonas aerogenosa* (D)

N	Tested bacteria	Inhibition zone diameter (mm) average ± SD			
		1	2	3	4
A	*Bacillus subtilis*	31 ± 0.52	32.5 ± 1	25 ± 0.5	28 ± 1.6
B	*Enterococcus sp.*	27 ± 1.78	40.5 ± 2.3	27 ± 1.75	31.5 ± 1
C	*E.coli*	26.4 ± 1	32 ± 1	20.5 ± 0.5	42 ± 2.73
D	*Pseudomonas aerogenosa*	23.45 ± 0.5	33.5 ± 1	20.5 ± 1	29.5 ± 2

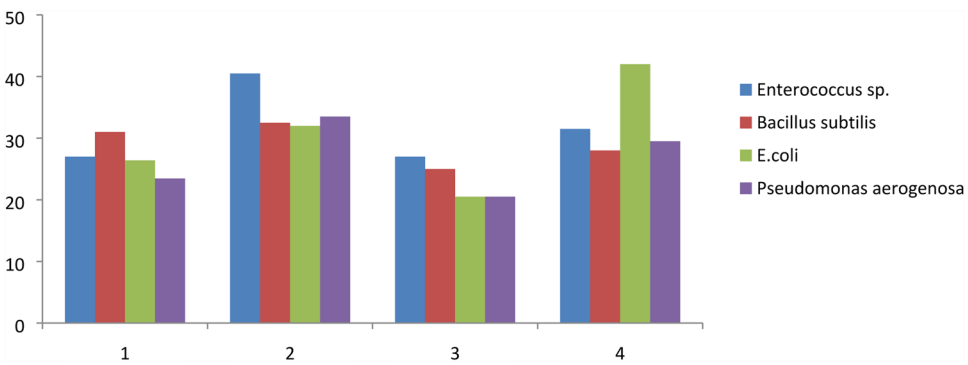

Fig. 6 Chart of antibacterial activity of materials 1, 2, 3, 4 tested against *Bacillus subtilis, Enterococcus sp.*, *E.coli* and *Pseudomonas aerogenosa*

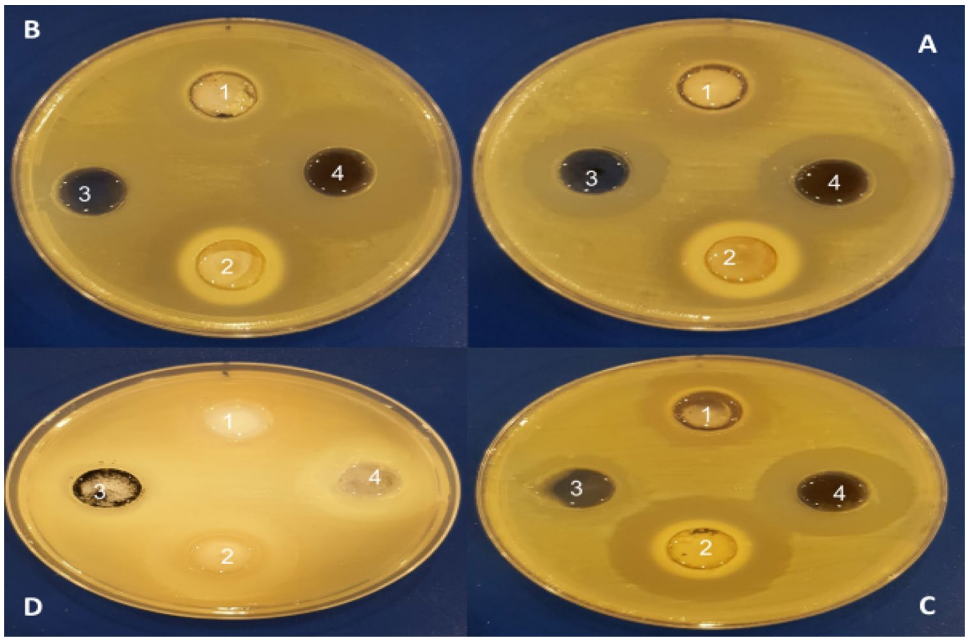

Fig. 7 Images of the results of the antibacterial test for materials 1, 2, 3, 4 against *Bacillus subtilis* (**a**), *Enterococcus sp.* (**b**), *E.coli* (**c**), and *Pseudomonas aerogenosa* (**d**) after 24 h incubation

Table 2 MIC values in (µg/mL) of materials 2 and 4 against *Bacillus subtilis* and *E. coli*

Inhibition zone diameter (mm)								
Material number	2				4			
Material concentration (µg/mL)	0.08	0.16	0.32	0.64	0.08	0.16	0.32	0.64
Bacillus subtilis	10	23	27	41	0	0	19	27
E. coli	10	12	16	40	0	0	10	30

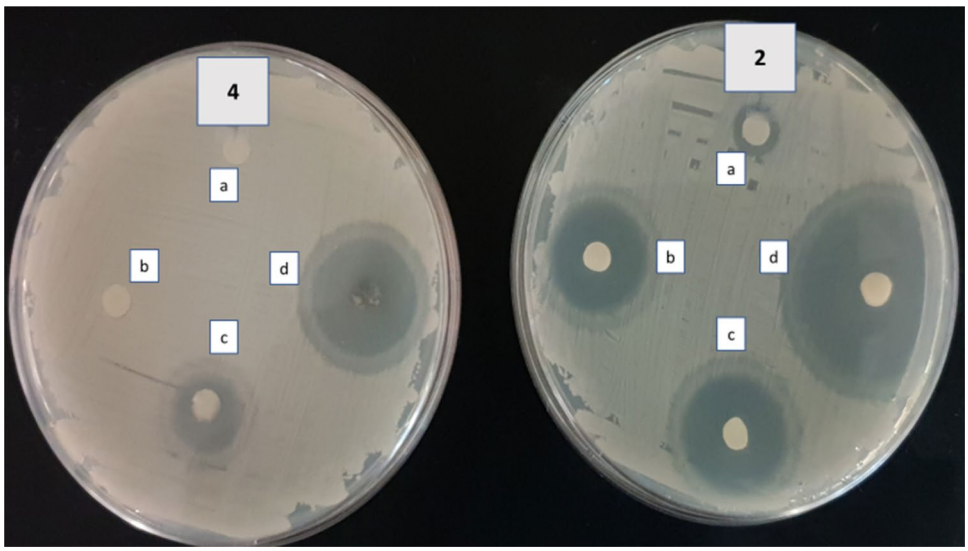

Fig. 8 Results of the antibacterial activity of 2 and 4 as determined by minimum inhibitory concentration (MIC) tested against *Bacillus subtilis* after 24 h incubation. **a**, **b**, **c**, **d** are abbriviations for concentrations of 0.08, 0.16, 0.32, and 0.64 (µg/mL), respectively

Conclusion

In the present work, a simple route for fabrication of core/shell CdO/Co_3O_4 mixed oxides and new composite Ag-NPs@CdO/Co_3O_4 by thermal degradation of oxalate precursors was discussed. The nanoparticles of precursors and composites were characterized by physicochemical techniques. The biological activity of the materials was analyzed in terms of the antibacterial activity against two

Gram-positive and two Gram-negative bacterial strains. High inhibition of bacterial growth was resulted from all tested materials particularly from materials contain silver in their structures which are exhibited higher antibacterial activity.

Acknowledgment The authors are thankful for Jouf University for supporting this work by chemicals, laboratories, and analysis.

Compliance with ethical standards

Competing interests No competing interest.

References

Abo Zeid EF, Ibrahem IA, Ali AM, Mohamed WA (2019) The effect of CdO content on the crystal structure, surface morphology, optical properties and photocatalytic efficiency of p-NiO/n-CdO nanocomposite. Results in Physics 12:562–570

Abo Zeid EF, Nassar AM, Hussein MA, Alam MM, Asiri AM, Hegazy HH, Rahman MM (2020) Mixed oxides CuO-NiO fabricated for selective detection of 2-aminophenol by electrochemical approach. J Mater Res Technol 9(2):1457–1467

Abureesh MA, Oladipo AA, Mizwari ZM, Berksel E (2018) Engineered mixed oxide-based polymeric composites for enhanced antimicrobial activity and sustained release of antiretroviral drug. Int J Biol Macromol 116:417–425

Alsohaimi IH, Nassar AM, Seaf Elnasr TA, Cheba BA (2020) A novel composite silver nanoparticles loaded calcium oxide stemming from egg shell recycling: A potent photocatalytic and antibacterial activities. J. Clen Prod 248:119274

Assim K, Schulze S, Pügner M, Uhlemann M, Gemming T, Giebeler L, Lang H (2017) Co (II) ethylene glycol carboxylates for Co_3O_4 nanoparticle and nanocomposite formation. J Mater Sci 52(11):6697–6711

Balamurugan S, Balu AR, Usharani K, Suganya M, Anitha S, Prabha D, Ilangovan S (2016) Synthesis of CdO nanopowders by a simple soft chemical method and evaluation of their antimicrobial activities. Pacific Sci Rev A: Nat Sci Eng 18(3):228–232

Basu T, Ghosh UC (2013) Nano-structured iron (III)–cerium (IV) mixed oxide: synthesis, characterization and arsenic sorption kinetics in the presence of co-existing ions aiming to apply for high arsenic groundwater treatment. Appl Surf Sci 283:471–481

Bayal N, Jeevanandam P (2012) Synthesis of CuO@ NiO core-shell nanoparticles by homogeneous precipitation method. J Alloy Compd 537:232–241

Du H, Wang J, Wang B, Cang D (2010) Preparation of cobalt oxalate powders with the presence of a pulsed electromagnetic field. Powder Technol 199(2):149–153

Elango M, Deepa M, Subramanian R, Saraswathy G (2018) Synthesis, structural characterization and antimicrobial activities of polyindole stabilized Ag-Co_3O_4 nanocomposite by reflux condensation method. Mater Chem Phys 216:305–315

Elseman AM, Shalan AE, Rashad MM, Hassan AM, Ibrahim NM, Nassar AM (2017) Easily attainable new approach to mass yield ferrocenyl Schiff base and different metal complexes of ferrocenyl Schiff base through convenient ultrasonication-solvothermal method. J Phys Org Chem 30(6):e3639

Fouad OA, Makhlouf SA, Ali GA, El-Sayed AY (2011) Cobalt/silica nanocomposite via thermal calcination-reduction of gel precursors. Mater Chem Phys 128(1–2):70–76

Gomes GA, da Costa GL, da Silva Figueiredo ABH (2018) Synthesis of ferrite nanoparticles Cu1− xAgxFe_2O_4 and evaluation of potential antibacterial activity. J Mater Res Technol 7(3):381–386

Gong P, Li H, He X, Wang K, Hu J, Tan W, Yang X (2007) Preparation and antibacterial activity of Fe3O4@ Ag nanoparticles. Nanotechnology 18(28):285604

Koohestani H (2019) Characterization of TiO2/WO3 composite produced with recycled WO3 nanoparticles from WNiFe alloy. Mater Chem Phys 229:251–256

Kooti M, Saiahi S, Motamedi H (2013) Fabrication of silver-coated cobalt ferrite nanocomposite and the study of its antibacterial activity. J Magn Magn Mater 333:138–143

Li Y, Tan B, Wu Y (2008) Mesoporous Co_3O_4 nanowire arrays for lithium ion batteries with high capacity and rate capability. Nano Lett 8(1):265–270

Li X, Zhu Z, Zhao Q, Wang L (2011) Photocatalytic degradation of gaseous toluene over ZnAl2O4 prepared by different methods: a comparative study. J Hazard Mater 186(2–3):2089–2096

Liu J, Wang Z, Luo Z, Bashir S (2013) Effective bactericidal performance of silver-decorated titania nano-composites. Dalton Trans 42(6):2158–2166

Makhlouf SA, Bakr ZH, Aly KI, Moustafa MS (2013) Structural, electrical and optical properties of Co_3O_4 nanoparticles. Superlattices Microstruct 64:107–117

Małecka B, Łącz A (2008) Thermal decomposition of cadmium formate in inert and oxidative atmosphere. Thermochim Acta 479(1–2):12–16

Manjula N, Pugalenthi M, Nagarethinam VS, Usharani K, Balu AR (2015) Effect of doping concentration on the structural, morphological, optical and electrical properties of Mn-doped CdO thin films. Mater Sci-Poland 33(4):774–781

Morones JR, Elechiguerra JL, Camacho A, Holt K, Kouri JB, Ramírez JT, Yacaman MJ (2005) The bactericidal effect of silver nanoparticles. Nanotechnology 16(10):2346

Nassar AM, Zeid EA, Elseman AM, Alotaibi NF (2018) A novel heterometallic compound for design and study of electrical properties of silver nanoparticles-decorated lead compounds. New J Chem 42(2):1387–1395

Nassar AM, Elseman AM, Alsohaimi IH, Alotaibi NF, Khan A (2019) Diaqua oxalato strontium (II) complex as a precursor for facile fabrication of Ag-NPs@ $SrCO_3$, characterization, optical properties, morphological studies and adsorption efficiency. J Coord Chem 72(5–7):771–785

Nayaka GP, Pai KV, Santhosh G, Manjanna J (2016) Recovery of cobalt as cobalt oxalate from spent lithium ion batteries by using glycine as leaching agent. J Environ Chem Eng 4(2):2378–2383

Perez C (1990) Antibiotic assay by agar-well diffusion method. Acta Biol Med Exp 15:113–115

Rai MK, Deshmukh SD, Ingle AP, Gade AK (2012) Silver nanoparticles: the powerful nanoweapon against multidrug-resistant bacteria. J Appl Microbiol 112(5):841–852

Raj AME, Jayanthi DD, Jothy VB (2008) Optimized growth and characterization of cadmium oxalate single crystals in silica gel. Solid State Sci 10(5):557–562

Ren YY, Yang H, Wang T, Wang C (2019) Bio-synthesis of silver nanoparticles with antibacterial activity. Mater Chem Phys 235:121746

Sadhukhan S, Ghosh TK, Roy I, Rana D, Bhattacharyya A, Saha R, Chattopadhyay D (2019) Green synthesis of cadmium oxide decorated reduced graphene oxide nanocomposites and its electrical and antibacterial properties. Mater Sci Eng, C 99:696–709

Sakthivel P, Asaithambi S, Karuppaiah M, Yuvakkumar R, Hayakawa Y, Ravi G (2020) Improved optoelectronic properties of Gd doped

cadmium oxide thin films through optimized film thickness for alternative TCO applications. J Alloy Compd 820:153188
Salam MA, Abu Khadra MR, Mohamed AS (2020) Effective oxidation of methyl parathion pesticide in water over recycled glass based-MCM-41 decorated by green Co3O4 nanoparticles. Environ Pollut 259:113874
Salem A (2014) Silver-doped cadmium oxide nanoparticles: synthesis, structural and optical properties. The Euro Physical J Plus 129(12):1–12
Sun L, Qiu K (2012) Organic oxalate as leachant and precipitant for the recovery of valuable metals from spent lithium-ion batteries. Waste Manage 32(8):1575–1582
Usharani K, Balu AR, Nagarethinam VS, Suganya M (2015) Characteristic analysis on the physical properties of nanostructured Mg-doped CdO thin films—doping concentration effect. Progress Nat Sci: Mater Int 25(3):251–257
Vennela AB, Mangalaraj D, Muthukumarasamy N, Agilan S, Hemalatha KV (2019) Structural and optical properties of Co_3O_4 nanoparticles prepared by sol-gel technique for photocatalytic application. Int J Electrochem Sci 14:3535–3552
Wang X, Yang Y, Zhang F, Tang J, Guo Z (2020) Facile synthesis of Co_3O_4/CdO nanospheres as high rate performance supercapacitors. Mater Lett 261:127141
Williams JM, Beno MA, Carlson KD, Geiser U, Kao HI, Kini AM, Thorn RJ (1988) High transition temperature inorganic oxide superconductors: synthesis, crystal structure, electrical properties, and electronic structure. Acc Chem Res 21(1):1–7
Yang W, Wang C, Arrighi V (2018) Silver oxalate ink with low sintering temperature and good electrical property. J Electron Mater 47(5):2824–2835
Yuan C, Wu HB, Xie Y, Lou XW (2014) Mixed transition-metal oxides: design, synthesis, and energy-related applications. Angew Chem Int Ed 53(6):1488–1504
Zahera M, Khan SA, Khan IA, Sharma RK, Sinha N, Al-Shwaiman HA, Khan MS (2020) Cadmium oxide nanoparticles: an attractive candidate for novel therapeutic approaches. Colloids Surf, A 585:124017
Zakrzewska K (2001) Mixed oxides as gas sensors. Thin Solid Films 391(2):229–238
Zou D, Xu C, Luo H, Wang L, Ying T (2008) Synthesis of Co3O4 nanoparticles via an ionic liquid-assisted methodology at room temperature. Mater Lett 62(12–13):1976–1978